Smart Structures and Systems, Vol. 5, No. 1 (2009) 23-42
DOI: http://dx.doi.org/10.12989/sss.2009.5.1.023

Static analysis of rubber components with piezoelectric patches using nonlinear finite element

M. C. Manna*

Department of Applied Mechanics, Bengal Engineering and Science University, Howrah–711 103, India

A. H. Sheikh

School of Civil, Environmental and Mining Engineering, The University of Adelaide, South – 5005, Australia

R. Bhattacharyya

Department of Mechanical Engineering, Indian Institute of Technology, Kharagpur – 721 302, India

(Received May 18, 2006, Accepted February 18, 2008)

Abstract. In order to reduce vibration or to control shape of structures made of metal or composites, piezoelectric materials have been extensively used since their discovery in 1880's. A recent trend is also seen to apply piezoelectric materials to flexible structures made of rubber-like materials. In this paper a non-linear finite element model using updated Lagrangian (UL) approach has been developed for static analysis of rubber-elastic material with surface-bonded piezoelectric patches. A compressible stain energy function has been used for modeling the rubber as hyperelastic material. For formulation of the nonlinear finite element model a twenty-node brick element is used. Four degrees of freedom u, v and w and electrical potential φ per node are considered as the field variables. PVDF (polyvinylidene fluoride) patches are applied as sensors/actuators or sensors and actuators. The present model has been applied to bimorph PVDF cantilever beam to validate the formulation. It is then applied to study the smart rubber components under different boundary and loading conditions. The results predicted by the present formulation are compared with the analytical solutions as well as the available published results. Some results are given as new ones as no published solutions available in the literatures to the best of the authors' knowledge.

Keywords: nonlinear finite element; compressible strain energy function; hyperelastic material; piezo-rubber beam; smart rubber beam.

1. Introduction

The use of rubber as structural material is gaining popularity steadily due to some of its specific features. One of the significant advantages of the material is its ability to dissipate kinetic energy associated with impact, shock or any dynamic loading, which is much higher compared to other materials. The material has a large amount of deformability and it is interesting that the elasticity is

*E-mail: mcm_naval@rediffmail.com

retained in that range of deformation if Mullin's effect and permanent set are ignored. These unique features are exploited to solve many engineering problems in an elegant manner. The use of rubber as vibration isolators, shock absorbers, load bearing materials, sealant materials and filler between two railway lines are some of its important applications. This specific aspect is well documented in the text by Gent (2001).

Discovery of the properties of piezoelectric materials by the Curie brothers in the 1880s has opened a new technique to control and suppress the vibration and deformation of structures. Electric charge is produced in piezoelectric material due to direct piezoelectric effect when it is subjected to a mechanical deformation and it gets deformed when a voltage is applied to it by virtue of converse piezoelectric effect. Of course, initially the utilization of piezoelectric materials was made in the field of ultrasonics. Later on in the early 1900's the advantage of these unique properties has been successfully engineered to different fields of science and technology. Olson (1956) was one of the many researchers who explained the uses of piezoelectric materials as vibration absorbers in vibration control of structural members. In general, the early references confine to piezoelectric actuation on concept demonstration rather than detailed modeling. The paper by Forward (1979) may be cited as one of the first papers on active damping using piezoelectric materials. Forward illustrated how piezoelectric materials could be used to add damping to flexible structures, but he did not concentrate on mechanical modeling of either the structure or the piezoelectric elements. Allik and Hughes (1970)were the first to present a finite element formulation for electroelastic analysis to incorporate the piezoelectric effect. They developed a three-dimensional tetrahedral finite element formulation that could be extended to derive electroelastic finite elements for one- and two-dimensional analysis.

Use of a thin polyvinylidene fluoride (PVDF) layer has been first proposed by Bailey and Hubbard (1985) for increasing damping of thin beams. They designed an active vibration damper for a cantilever beam using a distributed-parameter actuator (PVDF) and distributed-parameter control theory. They used Lyapunov's second method for distributed-parameter systems to design a control algorithm for the damper. Their analysis was applied to cantilever beams made of steel and aluminium. Fanson and Caughey (1987) demonstrated the technique of positive position feedback on a flexible beam using piezoelectric elements as collocated sensors and actuators. Crawley and de Luis (1987)proposed an analytical model for segmented piezoelectric actuators using Bernoulli-Euler beam theory for the analysis of piezoelectric actuators bonded to the surface or embedded in a laminate. They conducted the static and dynamic analyses on three specimens of cantilever beams of aluminium with surface-bonded actuators, glass/epoxy with two embedded actuators and glass/epoxy with a single embedded actuator. Park and Chopra (1996) modeled the actuation of piezoelectric patch with a beam in torsion. A one-dimensional beam model is used to determine the coupled extension/bending/torsion response to an applied voltage across the piezo-actuator. Detailed results are derived for a thin isotropic beam with a surface bonded piezoceramic actuator and compared to experiments. Lim, *et al.* (2001) conducted a three-dimensional analytical study for parallel piezo bimorph that are used as a sensor and actuator. A general analysis is done based on state space formulation combined with an asymptotic expansion technique. In this formulation three-dimensional solution to the bimorph generates directly by solving two-dimensional equations. Ye, *et al.* (2000) studied large deformation analysis of beams and plates using a nonlinear finite element method. Mukherjee and Saha Chaudhuri (2002) explored the demonstration of the effect of large deformation on piezoelectric materials and structures. They used an energy based electromechanical piezoelectric constitutive law derived by Tiersten (1969). For large deformation analysis of beams, a counterpart of Von Karman's plate equation is considered. The displacement based finite element formulation is derived using first order shear deformation theory (FOSDT). They have

conducted the nonlinear analysis of a bimorph beam made of PVDF under different loading conditions using Newton-Raphson iterative scheme. But all are limited to structures made of piezoelectric materials with conventional isotropic elastic materials. Applying displacement feedback and velocity feedback technique they have also explained a comprehensive formulation for instability control of piezolaminated imperfect struts made of steel and PZT layers using an imperfect approach under arbitrary dynamic excitation (2004). In this context, another study by Mukherjee and Saha Chaudhuri (2005) is worth mentioning where the exact solutions is presented and validated by experiments to show the effect of axial forces on smart columns made of plastic substrates and PVDF layers.

Modeling on piezoelectric material on rubbersubstrate has been attracting the researchers as rubber is gaining its practical applications in many engineering problems as tires, flexible pipes etc. As rubber is hyperelastic, near incompressible and undergoes large deformation which leads to geometric nonlinearity and its mechanical properties are characterized by a strain energy density function which results in nonlinear stress-strain relationship, it is very likely that creating a mathematical model of piezoelectric patches on rubber substrate by finite element method would be an arduous task. Austin and Ananthasayanam (2002) have attempted to study the effect of piezoelectric patches on the curvatures of rubber substrate due to the application of actuating voltage. They concentrated their studies on the linear analysis of the structure only. Since information available on the behavior of surface bonded piezoelectric patch/layer on a rubber-like substrate for static and dynamic behaviors is limited, in the present studya displacement based nonlinear finite element method is used for static shape control of flexible structures made of rubber substrate and the piezoelectric layers (PVDF). The focal point of the present work is to understand the piezoelectric effect on shape control of a rubber component considering geometric non-linearity for both rubber and piezoelectric materials and material non-linearity for rubber only.

2. Finite element formulation

In the analysis of smart rubber structures, the incremental solution scheme is most suitable as severe nonlinearity is involved in such analysis. In this solution scheme the entire loading path is divided into a number of steps. It gives different configurations/states such as ${}^{0}\Pi$, ${}^{1}\Pi$,..., ${}^{n}\Pi$, ${}^{n+1}\Pi$,..., where ${}^{0}\Pi$ is the initial state while ${}^{n}\Pi$ is any intermediate one. In this system any displacement component u_i and the electric potential φ at two adjacent statesof deformations may be expressed as

$$ {}^{n+1}u_i = {}^{n}u_i + u_i \quad (i = 1, 2, \text{and } 3), \; {}^{n+1}\varphi = {}^{n}\varphi + \varphi \tag{1} $$

where u_i and φ are the increment of the displacement component ${}^{n}u_i$ and the electric potential ${}^{n}\varphi$, respectively. In a similar manner the co-ordinates at any state may be obtained as

$$ {}^{n+1}x_i = {}^{0}x_i + {}^{n+1}u_i \text{ or } {}^{n+1}x_i = {}^{n}x_i + u_i \tag{2} $$

Now the equilibrium equation of the body at any state may be obtained using the principle of virtual work and the updated Lagrangian concept (Bathe 1996) as

$$ \int \delta({}^{n+1}_{n}\varepsilon)\, {}^{n+1}_{n}\sigma \, {}^{n}dV = {}^{n+1}P \tag{3} $$

where

$$ {}^{n+1}P = \int \delta({}^{n+1}u_k)\,{}^{n}\rho({}^{n+1}_{n}f_k)\,{}^{n}dV + \int \{\delta({}^{n+1}u_k)\,{}^{n+1}_{n}t_k + \delta({}^{n+1}\phi)\,{}^{n+1}_{n}Q\}\,{}^{n}dA \tag{4} $$

In the above Eqs. (3) and (4), $\delta({}^{n+1}_{n}\varepsilon)$ is the variation of Green-Lagrangian strain ${}^{n+1}_{n}\varepsilon$, ${}^{n+1}_{n}\sigma$ is the corresponding 2nd Piola Kirchhoff stress, ${}^{n}dV$ is the volume of an element, ${}^{n}\rho$ is the density at n-th configuration, ${}^{n+1}_{n}f_k$ is the body force per unit mass, ${}^{n+1}_{n}t_k$ is the deformation independent surface force, ${}^{n+1}_{n}Q$ is the surface charge and ${}^{n}dA$ is the surface area an element at n-th configuration. The left superscript denotes the configuration at which the quantity is to be considered whereas the left subscript denotes the configuration with respect to which the quantity is to be measured.

Now the above generalized stress and strain may be expressed with the help of incremental decomposition as follows:

$$ {}^{n+1}_{n}\sigma = {}^{n}_{n}\sigma + \sigma \tag{5} $$

$$ {}^{n+1}_{n}\varepsilon_{ij} = {}^{n}_{n}\varepsilon + \varepsilon \tag{6} $$

Since ${}^{n}_{n}\varepsilon = 0$ in the above equation, it may be expressed by splitting the incremental part ε into linear and nonlinear components as

$$ {}^{n+1}_{n}\varepsilon = \varepsilon = \varepsilon^{0} + \varepsilon^{L} \tag{7} $$

where

$$ \{\varepsilon^{0}\} = \{\varepsilon^{0}_{11}\ \varepsilon^{0}_{22}\ \varepsilon^{0}_{33}\ 2\varepsilon^{0}_{12}\ \varepsilon 2^{0}_{23}\ 2\varepsilon^{0}_{31}\ -E_1\ -E_2\ -E_3\}^{T} = \{\{\bar{\varepsilon}^{0}\}\{\bar{E}\}\}^{T} \tag{8} $$

$$ \{\varepsilon^{L}\} = \{\varepsilon^{L}_{11}\ \varepsilon^{L}_{22}\ \varepsilon^{L}_{33}\ 2\varepsilon^{L}_{12}\ \varepsilon 2^{L}_{23}\ 2\varepsilon^{L}_{31}\ 0\ 0\ 0\}^{T} = \{\{\bar{\varepsilon}^{L}\}\{0\}\}^{T} \tag{9} $$

$$ \varepsilon^{0}_{ij} = \frac{1}{2}\left(\frac{\partial u_i}{\partial({}^{n}x_j)} + \frac{\partial u_j}{\partial({}^{n}x_i)}\right),\quad E_i = -\frac{\partial \phi}{\partial({}^{n}x_j)} \text{ and } \varepsilon^{L}_{ij} = \frac{1}{2}\left(\frac{\partial u_k}{\partial({}^{n}x_i)}\frac{\partial u_k}{\partial({}^{n}x_j)}\right) \tag{10} $$

Again ${}^{n}_{n}\sigma$ is simply the generalized Cauchy stress ${}^{n}\tau$ and with this Eq. (5) becomes

$$ {}^{n+1}_{n}\sigma = {}^{n}\tau + \sigma \tag{11} $$

where

$$ {}^{n}\tau = \{{}^{n}\underset{\sim}{\tau}_{11}\ {}^{n}\underset{\sim}{\tau}_{22}\ {}^{n}\underset{\sim}{\tau}_{33}\ {}^{n}\underset{\sim}{\tau}_{12}\ {}^{n}\underset{\sim}{\tau}_{23}\ {}^{n}\underset{\sim}{\tau}_{31}\ {}^{n}D_1\ {}^{n}D_2\ {}^{n}D_3\}^{T} = [\{{}^{n}\underset{\sim}{\tau}\}^{T}\{{}^{n}D\}^{T}] \tag{12} $$

$$ \sigma = \{\sigma_{11}\ \sigma_{22}\ \sigma_{33}\ \sigma_{12}\ \sigma_{23}\ \sigma_{31}\ D_1\ D_2\ D_3\}^{T} = [\{\underset{\sim}{\sigma}\}^{T}\{D\}^{T}] \tag{13} $$

The generalized Cauchy stress ${}^{n}\tau$ and the incremental stress σ inthe above equation may be obtained as:

$$ \begin{bmatrix} \{{}^{n}\underset{\sim}{\tau}\} \\ \{{}^{n}D\} \end{bmatrix} = \begin{bmatrix} {}_{n}\hat{C} & {}_{n}\hat{e} \\ {}_{n}\hat{e}^{T} & -{}_{n}\hat{\underset{\sim}{\varrho}} \end{bmatrix} \begin{Bmatrix} {}^{n}\underset{\sim}{\varepsilon} \\ {}^{n}E \end{Bmatrix} = [{}_{n}\bar{C}]\{{}^{n}\varepsilon\} \tag{14} $$

$$\begin{bmatrix}\{\sigma\}\\ \{D\}\end{bmatrix} = \begin{bmatrix}{}_n\hat{C} & {}_n\hat{e}\\ {}_n\hat{e}^T & -{}_n\hat{\wp}\end{bmatrix}\begin{Bmatrix}\varepsilon\\ E\end{Bmatrix} = [{}_n\bar{C}]\{\varepsilon\} \tag{15}$$

In the above Eqs. (10) and (11), the constitutive tensor $[\bar{C}]$ and the Almansi strain tensor $\{{}^n\varepsilon\}$ can be obtained from the relationships as

$$[{}_n\bar{C}] = \begin{bmatrix}[T_m]^{-1} & 0\\ 0 & [T_e]^{-1}\end{bmatrix}\begin{bmatrix}[{}_nC] & [{}_ne]\\ [{}_ne]^T & -[{}_n\wp]\end{bmatrix}\begin{bmatrix}[T_m]^{-1} & 0\\ 0 & [T_e]^{-T}\end{bmatrix} \tag{16}$$

where $[{}_ne]$ is the piezoelectric stress matrix, $[{}_n\wp]$ is the dielectric constant matrix, $[T_m]$ and $[T_e]$ are the coordinate transformation matrices from material Cartesian coordinates to global Cartesian coordinates for strain and electric field vectors respectively and $[{}_nC]$ is the constitutive tensor and

$$\{{}^n\varepsilon\} = \{{}^n\varepsilon_{11}\ {}^n\varepsilon_{22}\ {}^n\varepsilon_{33}\ 2^n\varepsilon_{12}\ 2^n\varepsilon_{23}\ 2^n\varepsilon_{31}\ -{}^nE_1\ -{}^nE_2\ -{}^nE_3\}^T \tag{17}$$

where

$${}^n\varepsilon_{kl} = \frac{1}{2}\left(\frac{\partial({}^nu_k)}{\partial({}^nx_l)} + \frac{\partial({}^nu_l)}{\partial({}^nx_k)} - \frac{\partial({}^nu_r)}{\partial({}^nx_k)}\frac{\partial({}^nu_r)}{\partial({}^nx_l)}\right) \tag{18}$$

$${}^nE_k = -\frac{\partial({}^n\phi)}{\partial({}^nx_k)} \tag{19}$$

$$[{}_ne] = \begin{bmatrix}{}_ne_{11} & {}_ne_{12} & {}_ne_{13} & {}_ne_{14} & {}_ne_{15} & {}_ne_{16}\\ {}_ne_{21} & {}_ne_{22} & {}_ne_{23} & {}_ne_{24} & {}_ne_{25} & {}_ne_{26}\\ {}_ne_{31} & {}_ne_{32} & {}_ne_{33} & {}_ne_{34} & {}_ne_{35} & {}_ne_{36}\end{bmatrix}^T \tag{20}$$

$$[{}_n\wp] = \begin{bmatrix}{}_n\wp_1 & 0 & 0\\ 0 & {}_n\wp_2 & 0\\ 0 & 0 & {}_n\wp_3\end{bmatrix} \tag{21}$$

For rubber material, ${}_n\hat{C}$ is obtained from its strain energy density function to be presented later (Bathe 1996) and $[{}_ne]$ and $[{}_n\wp]$ are piezoelectric constant matrix and dielectric constant matrices, respectively.

Substitution of Eqs. (7), (11) and (15) in Eq. (3) gives

$$\int\delta(\varepsilon)_n\bar{C}\varepsilon\,{}^ndV + \int\delta(\varepsilon^L)^n\tau\,{}^ndV = {}^{n+1}P - \int\delta(\varepsilon^0)^n\tau\,{}^ndV \tag{22}$$

Since it is not possible to solve the above equation due to the presence of nonlinear incremental strains, it is linearized by taking $\delta(\varepsilon) = \delta(\varepsilon^0)$ and $\varepsilon = \varepsilon^0$ to get an approximate solution. With these the Eq. (22) becomes

$$\int\delta(\varepsilon^0)_n\bar{C}\varepsilon^0\,{}^ndV + \int\delta(\varepsilon^L)^n\tau\,{}^ndV = {}^{n+1}P - \int\delta(\varepsilon^0)^n\tau\,{}^ndV \tag{23}$$

Since $\delta({}^{n+1}u_k) = \delta(u_k)$ and $\delta({}^{n+1}\phi) = \delta(\phi)$, the virtual work due to external loads ${}^{n+1}P$ presented

in (4) may be rewritten as

$$ {}^{n+1}P = \int \delta(u_k)\,{}^{n}\rho({}^{n+1}_{n}f_k)\,{}^{n}dV + \int \{\delta(u_k)\,{}^{n+1}_{n}t_k + \delta(\phi)\,{}^{n+1}_{n}Q\}\,{}^{n}dA \tag{24} $$

Eqs. (22) and (23) may be expressed with the help of Eqs. (8), (9) and (10) as

$$ \int \delta\{\varepsilon^0\}^T [{}_{n}\bar{C}]\{\varepsilon^0\}\,{}^{n}dV + \int \delta\{\theta\}^T [{}^{n}\bar{\tau}]\{\theta\}\,{}^{n}dV = {}^{n+1}P - \int \delta\{\varepsilon^0\}^T \{{}^{n}\tau\}\,{}^{n}dV \tag{25} $$

and

$$ {}^{n+1}P = \int \delta\{\bar{u}\}^T\,{}^{n}\rho\{{}^{n+1}_{n}\bar{f}\}\,{}^{n}dV + \int \{\delta\{\bar{u}\}\{{}^{n+1}_{n}\bar{t}\} + \delta(\phi)\,{}^{n+1}_{n}Q\}\,{}^{n}dA \tag{26} $$

where the different matrices in the above Eqs. (25) and (26) are:

$$ \{\bar{u}\} = \{u_1\ u_2\ u_3\}^T \tag{27} $$

$$ \{{}^{n+1}_{n}\bar{f}\} = \{{}^{n+1}_{n}f_1\ \ {}^{n+1}_{n}f_2\ \ {}^{n+1}_{n}f_3\}^T \tag{28} $$

$$ \{{}^{n+1}_{n}\bar{t}\} = \{{}^{n+1}_{n}t_1\ \ {}^{n+1}_{n}t_2\ \ {}^{n+1}_{n}t_3\}^T \tag{29} $$

$$ \{\theta\} = \left\{ \frac{\partial u_1}{\partial({}^{n}x_1)} \frac{\partial u_1}{\partial({}^{n}x_2)} \frac{\partial u_1}{\partial({}^{n}x_3)} \frac{\partial u_2}{\partial({}^{n}x_1)} \frac{\partial u_2}{\partial({}^{n}x_2)} \frac{\partial u_2}{\partial({}^{n}x_3)} \frac{\partial u_3}{\partial({}^{n}x_1)} \frac{\partial u_3}{\partial({}^{n}x_2)} \frac{\partial u_3}{\partial({}^{n}x_3)} \right\}^T \tag{30} $$

$$ [{}^{n}\bar{\tau}] = \begin{bmatrix} [{}^{n}\tilde{\tau}] & 0 & 0 \\ 0 & [{}^{n}\tilde{\tau}] & 0 \\ 0 & 0 & [{}^{n}\tilde{\tau}] \end{bmatrix}, \quad [{}^{n}\tilde{\tau}] = \begin{bmatrix} {}^{n}\tau_{11} & {}^{n}\tau_{12} & {}^{n}\tau_{13} \\ {}^{n}\tau_{21} & {}^{n}\tau_{22} & {}^{n}\tau_{23} \\ {}^{n}\tau_{31} & {}^{n}\tau_{32} & {}^{n}\tau_{33} \end{bmatrix} \tag{31} $$

Now Eqs. (19) and (20) are in convenient form for its finite element implementation, where the twenty noded 3D brick element (Fig. 1) based on isoparametric formulation is used. According to isoparametric formulation the displacements, geometry and electrical potential at *n*-th configuration can be represented with same interpolation functions (Bathe 1996) as

$$ {}^{n}x_i = \sum_{k=1}^{20} N^k(\xi, \eta, \zeta)\,{}^{n}x_i^k, \quad {}^{n}u_i = \sum_{k=1}^{20} N^k(\xi, \eta, \zeta)\,{}^{n}u_i^k, \quad {}^{n}\phi = \sum_{k=1}^{20} N^k(\xi, \eta, \zeta)\,{}^{n}\phi^k \tag{32} $$

where $N^k(\xi, \eta, \zeta)$ or simply N^k is the interpolation function corresponding to *k*-th node, while ${}^{n}x_i^k$, ${}^{n}u_i^k$ and ${}^{n}\phi^k$ are the coordinate, displacement and electrical potential at the corresponding node, respectively. In a similar manner the incremental displacements and the incremental electrical potential ϕ can be expressed as

$$ u_i = \sum_{k=1}^{20} N^k u_i^k \text{ and } \phi = \sum_{k=1}^{20} N^k \phi^k \tag{33} $$

With Eqs. (32) and (33) along with (8-10), the incremental strain vectors $\{\bar{\varepsilon}^0\}$ and $\{\theta\}$ in (25) and incremental displacement vector $\{\bar{u}\}$ in (26) may be expressed in terms of incremental nodal

displacement vector $\{U\}$ as

$$\{\bar{\varepsilon}^0\} = [[B_0^1]\ [B_0^2]\ [B_0^3]\cdots[B_0^k]\cdots[B_0^{20}]] = [B_0]\{\bar{U}\} \tag{34}$$

$$\{\bar{E}\} = [[B_\phi^1]\ [B_\phi^2]\ [B_\phi^3]\cdots[B_\phi^k]\cdots[B_\phi^{20}]] = [B_\phi]\{\bar{\phi}\} \tag{35}$$

$$\{\theta\} = [[B_G^1]\ [B_G^2]\ [B_G^3]\cdots[B_G^k]\cdots[B_G^{20}]] = [B_G]\{\bar{U}\} \tag{36}$$

$$\{\bar{u}\} = [[N_u^1]\ [N_u^2]\ [N_u^3]\cdots[N_u^k]\cdots[N_u^{20}]] = [N_u]\{\bar{U}\} \tag{37}$$

$$\{\phi\} = [N^1\ \ N^2\ \ \cdots\cdots\ N^{20}]\{\bar{\phi}\} = [N_\phi]\{\bar{\phi}\} \tag{38}$$

where

$$\{\bar{U}\} = \{u_1^1\ \ u_2^1\ \ u_3^1\ \ u_1^2\ \ u_2^2\ \ u_3^2\cdots\cdots\ u_1^{20}\ \ u_2^{20}\ \ u_3^{20}\}^T \tag{39}$$

$$\{\bar{\phi}\} = [\phi^1\ \ \phi^2\ \ \cdots\cdots\ \phi^{20}]^T \tag{40}$$

$$[B_0^k] = \begin{bmatrix} \dfrac{\partial N^k}{\partial^n x_1} & 0 & 0 & \dfrac{\partial N^k}{\partial^n x_2} & 0 & \dfrac{\partial N^k}{\partial^n x_3} \\ 0 & \dfrac{\partial N^k}{\partial^n x_2} & 0 & \dfrac{\partial N^k}{\partial^n x_1} & \dfrac{\partial N^k}{\partial^n x_3} & 0 \\ 0 & 0 & \dfrac{\partial N^k}{\partial^n x_3} & 0 & \dfrac{\partial N^k}{\partial^n x_2} & \dfrac{\partial N^k}{\partial^n x_1} \end{bmatrix} \tag{41}$$

$$[B_\phi^k] = \begin{bmatrix} \dfrac{\partial N^k}{\partial^n x_1} & \dfrac{\partial N^k}{\partial^n x_2} & \dfrac{\partial N^k}{\partial^n x_3} \end{bmatrix}^T \tag{42}$$

$$[B_G^k] = \begin{bmatrix} \dfrac{\partial N^k}{\partial^n x_1} & \dfrac{\partial N^k}{\partial^n x_2} & \dfrac{\partial N^k}{\partial^n x_3} & 0 & 0 & 0 & 0 & 0 & 0 \\ 0 & 0 & 0 & \dfrac{\partial N^k}{\partial^n x_1} & \dfrac{\partial N^k}{\partial^n x_2} & \dfrac{\partial N^k}{\partial^n x_3} & 0 & 0 & 0 \\ 0 & 0 & 0 & 0 & 0 & 0 & \dfrac{\partial N^k}{\partial^n x_1} & \dfrac{\partial N^k}{\partial^n x_2} & \dfrac{\partial N^k}{\partial^n x_3} \end{bmatrix}^T \tag{43}$$

$$[N_u^k] = \begin{bmatrix} N^k & 0 & 0 \\ 0 & N^k & 0 \\ 0 & 0 & N^k \end{bmatrix} \tag{44}$$

Substitution of Eqs. (34)-(38) in Eqs. (25) and (26) and performing necessary rearrangement the incremental equilibrium equation may be obtained in its final form as

$$[K_T]\{U\} = \{^{n+1}R\} - \{^{n+1}F\} \tag{45}$$

where

$$\{U\} = \begin{bmatrix} \{\bar{U}\}^T \\ \{\bar{\phi}\}^T \end{bmatrix} \tag{46}$$

$$[K_T] = \int \left(\begin{bmatrix} B_0 & 0 \\ 0 & B_\phi \end{bmatrix}^T [{}_n\bar{C}] \begin{bmatrix} B_0 & 0 \\ 0 & B_\phi \end{bmatrix} + \begin{bmatrix} B_G^{T\,n}\bar{\tau} B_G & 0 \\ 0 & 0 \end{bmatrix} \right) {}^n dV \tag{47}$$

$$\{^{n+1}R\} = \int \begin{bmatrix} N_u^T & 0 \\ 0 & N_\phi^T \end{bmatrix} {}^n\rho \begin{Bmatrix} {}^{n+1}_{n}\bar{f} \\ 0 \end{Bmatrix} {}^n dV + \int \begin{bmatrix} N_u^T & 0 \\ 0 & N_\phi^T \end{bmatrix} \begin{Bmatrix} {}^{n+1}_{n}\bar{t} \\ {}^{n+1}_{n}Q \end{Bmatrix} {}^n dV \tag{48}$$

$$\{^{n+1}F\} = \int \begin{bmatrix} B_0 & 0 \\ 0 & B_\phi \end{bmatrix}^T \{^n\tau\}\, {}^n dV \tag{49}$$

Following the usual technique, one may carry out numerical integration of these quantities according to Gauss quadrature integration rule where number of Gauss points taken in all the three directions is 3 before finally solving Eq. (45) by applying the arc-length method (Crisfield 1981).

Now the technique to evaluate the components of constitutive tensor ${}_nC_{ijkl}$ of rubber material is presented. In the present study the material models used are neo-Hookian, Mooney-Rivlin and Ogden-Tschoegl. In this context the strain energy density function W of Peng and Chang (1997), which may be expressed in terms of principal stretches (λ_1, λ_2, λ_3) as

$$W = \sum_{k=1}^{m} \mu_k \left(\frac{\lambda_1^{\alpha_k} + \lambda_2^{\alpha_k} + \lambda_3^{\alpha_k} - 3}{\alpha_k} - \ln J \right) + \frac{\lambda}{81}(9 \ln J + J^{-9} - 1) \tag{50}$$

where μ_k and α_k are material constants, $J = \lambda_1\lambda_2\lambda_3$, $m = 1, 2$ or 3 depending on the material model (Bathe 1996, Ogden 1984) and the Lame's constant $\lambda = 2G\nu/(1-2\nu) = \mu_k\alpha_k\nu/(1-2\nu)$. The values of principal stretches λ_i and their directions v_{ij} are obtained from the left Cauchy-Green deformation tensor $[B]$ defined in terms of deformation gradient tensor $[{}^n_0X]$ as

$$[B] = [{}^n_0X][{}^n_0X]^T \tag{51}$$

where

$$[{}^n_0X] = \begin{bmatrix} \dfrac{\partial^n x_1}{\partial^0 x_1} & \dfrac{\partial^n x_1}{\partial^0 x_2} & \dfrac{\partial^n x_1}{\partial^0 x_3} \\ \dfrac{\partial^n x_2}{\partial^0 x_1} & \dfrac{\partial^n x_2}{\partial^0 x_2} & \dfrac{\partial^n x_2}{\partial^0 x_3} \\ \dfrac{\partial^n x_3}{\partial^0 x_1} & \dfrac{\partial^n x_3}{\partial^0 x_2} & \dfrac{\partial^n x_3}{\partial^0 x_3} \end{bmatrix} \tag{52}$$

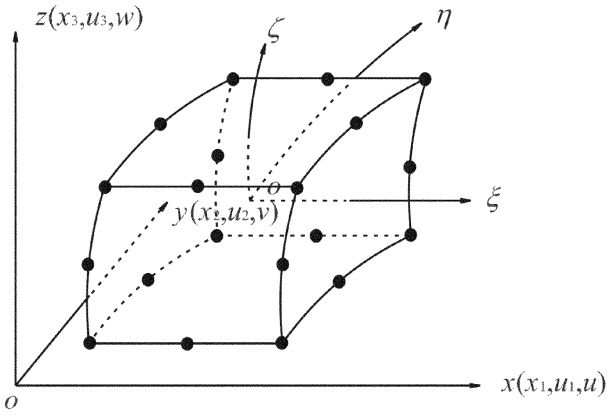

Fig. 1 Twenty noded 3D brick element

The matrix $[B]$ may be expressed in terms of the principal stretches λ_i and their directions v_{ij} as

$$[B] = \begin{bmatrix} v_{11} & v_{21} & v_{31} \\ v_{12} & v_{22} & v_{32} \\ v_{13} & v_{23} & v_{33} \end{bmatrix} \begin{bmatrix} \lambda_1^2 & 0 & 0 \\ 0 & \lambda_2^2 & 0 \\ 0 & 0 & \lambda_3^2 \end{bmatrix} \begin{bmatrix} v_{11} & v_{12} & v_{13} \\ v_{21} & v_{22} & v_{23} \\ v_{31} & v_{32} & v_{33} \end{bmatrix} = [v][L][v]^T \tag{53}$$

where $[v]$ and $[L]$ are the eigenvector and eigenvalue matrices respectively of $[B]$.

From the strain energy density function W in Eq. (50), the principal values of the Cauchy stress can be obtained (Ogden 1984) as

$${}^n t_i = \frac{\lambda_i}{J}\frac{\partial W}{\partial \lambda_i} = \frac{1}{J}\sum_{k=1}^{m} \mu_k(\lambda_i^{\alpha_k} - 1) + \frac{\lambda}{9}\left(\frac{1}{J} - \frac{1}{J^{10}}\right) \tag{54}$$

Using the Eqs. (50) and (53), for the components of constitutive tensor ${}_nC_{ijkl}$ one may obtain

$${}_nC_{ijkl} = \sum_{p=1}^{3}\sum_{q=1}^{3}\sum_{r=1}^{3}\sum_{s=1}^{3} v_{ip}v_{jq}L_{pqrs}v_{kr}v_{ls} \tag{55}$$

where, ${}_nL_{kkkk} = \lambda_k\frac{\partial^n t_k}{\partial \lambda_k} - {}^n t_k$, ${}_nL_{kkjj} = \lambda_j\frac{\partial^n t_k}{\partial \lambda_j} + {}^n t_k$, ${}_nL_{klkl} = \frac{{}^n t_k\lambda_1^2 - {}^n t_l\lambda_k^2}{\lambda_k^2 - \lambda_l^2}$ for $\lambda_k^2 \neq \lambda_l^2$ and ${}_nL_{klkl} = \frac{1}{2J}\sum_{i=1}^{m}\mu_i\alpha_i\lambda_k^{\alpha_i} - {}^n t_k$ for $\lambda_k^2 = \lambda_l^2$.

3. Results and discussions

In this section numerical examples of rubber components with piezoelectric patches are solved by the proposed finite element model to check its accuracyand range of applicability. For the purpose of validation, the analysis is first carried out on a cantilever PVDF bimorph beam subjected to different

Table 1 Material constants of different material models (Manna, *et al*. 2006)

Material model	m	μ_1 (MPa)	μ_2 (MPa)	μ_3 (MPa)	α_1	α_2	α_3	ν
Neo-Hookean	1	0.3924	0.0	0.0	2.0	0.0	0.0	0.49932
Mooney-Rivlin	2	0.367	-0.0292	0.0	2.0	-2.0	0.0	0.49932
Ogden-Tschoegl	3	0.618	0.001245	-0.00982	1.3	5.0	-2.0	0.49932

Table 2 Material constants of different isotropic materials (mukherjee and saha chaudhuri 2002)

Piezoelectric materials	Material constants	
PVDF	Elastic constant, E (GPa)	2.0
	Poisson's ratio, ν	0.29
	Density, ρ (kg/m^3)	1800
	Piezoelectric stress coefficient, e_{31} (C/m^2)	0.046
	Dielectricity, $\mathfrak{L}_3$ (F/m)	1.062×10^{-10}
	Maximum operating voltage (V/μm)	30
Steel	Elastic constant, E (GPa)	197.0
	Poisson's ratio, ν	0.33

applied voltages to see its actuation effect and a combination of transverse and compressive point loads at the free end to see the geometric nonlinear effect on the sensed voltages. The results obtained in all these cases are compared with the analytical solution and the results available in the literatures. Finally examples of smart rubber components are studied and results obtained are presented in graphical form as new results. In most of the cases the Ogden-Tschoegl, Mooney-Rivlin and neo-Hookean material models are used for rubber as in our previous paper (Manna, *et al*. 2006) where rubber/hyperelastic members have been analyzed under different modes of deformation using a twenty-node brick element. Unless specified various constants appearing in Eqs. (50) and (54) as shown in Table 1 are used in the present analysis. Different material properties of piezoelectric material and steel are also given in Table 2.

3.1. Cantilever bimorph beam

To validate the performance of the present formulation, static linear analysis of a PVDF bimorph cantilever beam (Fig. 2) is performed for different applied voltages. The results from linear static analysis have been presented in Tables 3 and 4 with those by Cheng, *et al*. (1997) and Tseng (1989)for comparison. The results compare well with the published available results. The results for present work for nonlinear analysis have been depicted in Figure 3 as new results. It has been found that the effect of geometric nonlinearity is prominent for high value of applied voltages as the deflection due to actuation effect for low voltages is too small to invoke the geometric nonlinearity. The tip deflection and the sensed voltage at fixed end of the beam for a transverse tip load of 0.025 N and a compressive axial load of 0.1 N are shown in Figs. 4 and 5 with those by Mukherjee and Saha Chowdhuri (2002). The tip deflection agrees well with those by Mukherjee and Saha Chowdhuri (2002). But the sensed voltages at the fixed end of the bimorph beam differ for nonlinear analysis whereas those show close agreement for linear analysis. Of course, the deviation is marginal and this may be due to the difference in approach of the present finite element formulation.In the present investigation the electrical potential is condensed to form element stiffness matrix and multipoint constraints are imposed on the top and bottom surfaces

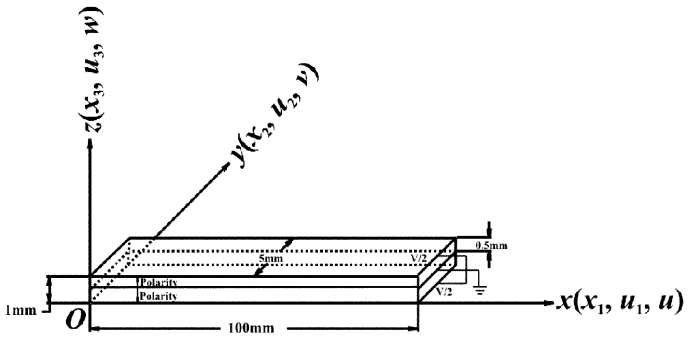

Fig. 2 Bimorph cantilever beam

Table 3 Tip deflection of a PVDF bimorph cantilever beam (for a unit voltage)

Distance (mm)	Theory (μm)	Chen, *et al.*(1997)	Tseng (1989)	Present analysis (linear)
20	0.0140	0.0139	0.0150	0.0134
40	0.0552	0.0547	0.0569	0.0542
60	0.1224	0.1135	0.1371	0.1226
80	0.2208	0.2198	0.2351	0.2185
100	0.3451	0.3416	0.3598	0.3420

Table 4 Tip deflection of a PVDF bimorph cantilever beam (for various voltages)

Voltage (V)	Theory (m)	Chen, *et al.* (1997) (m)	Tseng (1989) (m)	Present analysis (linear) (m)
50	0.1725×10^{-4}	0.1755×10^{-4}	0.1570×10^{-4}	0.1710×10^{-4}
100	0.3451×10^{-4}	0.3409×10^{-4}	0.3200×10^{-4}	0.3420×10^{-4}
150	0.5175×10^{-4}	0.5067×10^{-4}	0.4897×10^{-4}	0.5130×10^{-4}
200	0.6900×10^{-4}	0.6819×10^{-4}	0.6417×10^{-4}	0.6840×10^{-4}

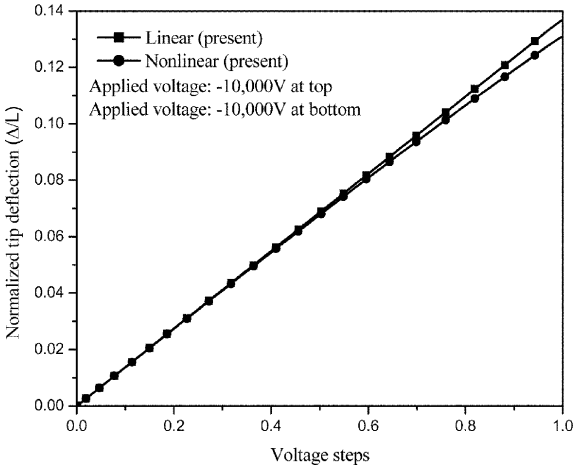

Fig. 3 Non-dimensional tip deflection of a PVDF bimorph beam for different applied voltages

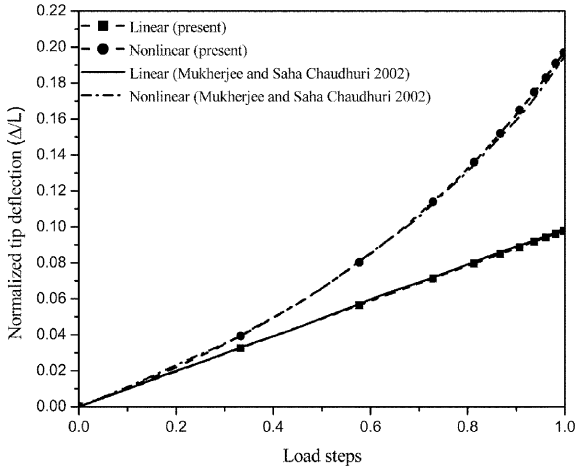

Fig. 4 Tip deflection of a PVDF bimorph beam

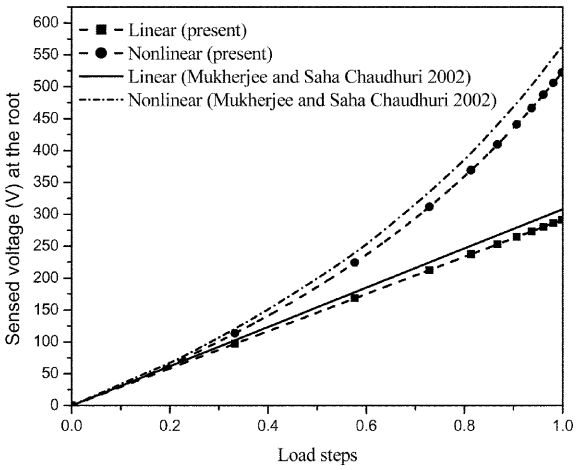

Fig. 5 Sensed voltage at the fixed end of a PVDF bimorph beam

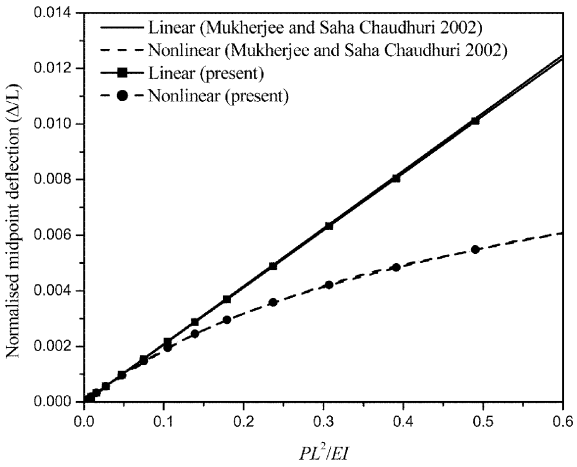

Fig. 6 Normalized midpoint deflection of both end pinned PVDF beam

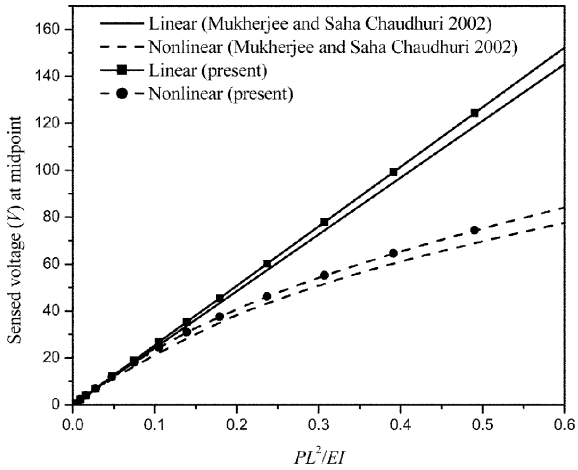

Fig. 7 Sensed voltages (V) at midpoint of both end pinned PVDF beam

of the piezoelectric layers. The piezoelectric layers are divided into segments equal to the number of elements when the piezoelectric layers are used as sensors. The sensed voltages are determined from the secant stiffness matrix which is unsymmetrical after converting it into a symmetric one (Wood and Schrefler 1978). Also the same bimorph beam is studied under the boundary conditions of both end pinned. The normalized midpoint deflection and the sensed voltage developed at the midpoint of the beam are plotted against the non-dimensional parameter (PL^2/EI) in Figs. 6 and 7. The deflections predicted by the present formulation are exactly matching with those by Mukherjee and Saha Chowdhuri (2002) whereas the sensed voltages are comparable with their results. In each case the beam is divided into 40 elements (mesh size is taken as 20×1×2).

3.2. Piezoelectric patch(PVDF) on rubber substrate

In this example, the static deformation of a neo-Hookean rubber beam with piezoelectric patches

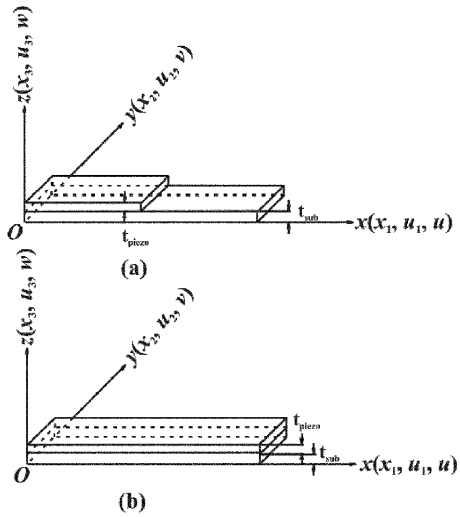

Fig. 8 Rubber substrate (a) with half span (b) with full span piezoelectric layer.

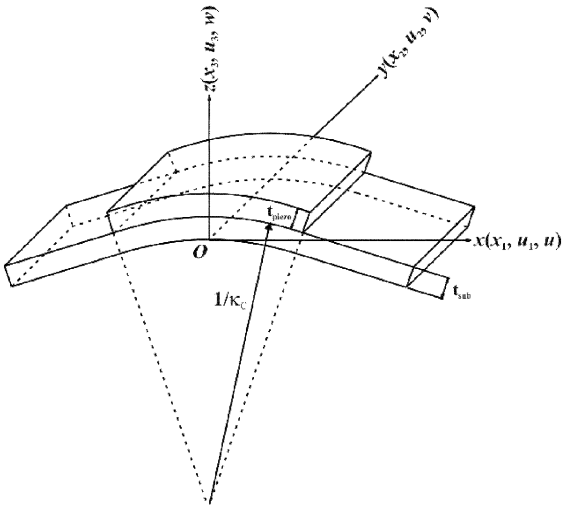

Fig. 9 Curvature definition

(PVDF) of half and full span (Fig. 8) is investigated with applied unit voltage at the external surface and zero potential at the piezo-rubber interface. The analysis is performed without considering geometric and material nonlinearities for the purpose of validation. The rubber-piezoelectric system is analyzed by assuming plain strain in the *y*-direction. Two cases with modulus ratios $E_{sub}=E_{piezo} = 1.0$ and $E_{sub}=E_{piezo} = 7.45\times10^{-5}$ are taken as from Austin and Ananthasayanam (2002)for the purpose of comparison with FE analysis, where subscript '*sub*' and '*piezo*' are used to denote substrate and piezoelectric layers, respectively. In the present study the value of E_{piezo} is used from Table 2 and the corresponding E_{sub} is found from the ratios. Notice that in the second case, the value of E_{sub} calculated from the ratio is very close to the value of Young's modulus for rubber material considered in Table 1. In both the cases the rubber substrate is divided into 80 elements (mesh size: 20×1×4) and the piezoelectric patch is divided into 20 elements (mesh size: 20×1×1) for full span and 10 elements (mesh size: 10×1×1) for half span patches. The length, width and thickness of the rubber substrate are 0.1m, 0.002m and 0.01 m, respectively. The boundary conditions are: $u_1 = u_2 = u_3 = 0$ and $x = 0$ and $u_2 = 0$ at $y = 0$ and $y = 2$ mm. The radius of curvature $1/\kappa_c$, where κ_c is the curvature, is shown in Fig. 9. From the Figs. 10 and 11 it may be observed that when the modulus ratio (Young's modulus of rubber/ Young's modulus of PVDF) is equal to one, the normalized curvature $(\kappa_c t_{sub}/2\Delta)$[1] obtained from the beams with half span and full span piezoelectric patches matches very closely with each other as well as with those given by Austin and Ananthasayanam (2002). When the above modulus ratio is very small, i.e. when there is high mismatch between the Young's moduli of thesubstrate and the piezoelectric patch, the beam with full span piezoelectric patch gives closer results compared to those by Austin and Ananthasayanam (2002). Also it is observed from Fig. 11 that there is no significant influence of the length of piezoelectric patch on the curvature irrespective of the thickness ratio. Note that the results obtained for $E_{sub} = E_{piezo} = 1.0$ (Fig. 10) there exists a maximum value of the curvature at about $t_{sub}/t_{piezo} = 2.0$ for which the normalized curvature approximately reads as 0.425. However, for $E_{sub} = E_{piezo} = 7.45\times10^{-5}$, the curvature increases monotonically with thickness ratio.

[1] $\Delta = V\, d_{31}/t_{piezo}$ where V and d_{31} are the applied voltage and the piezoelectric strain constant, respectively.

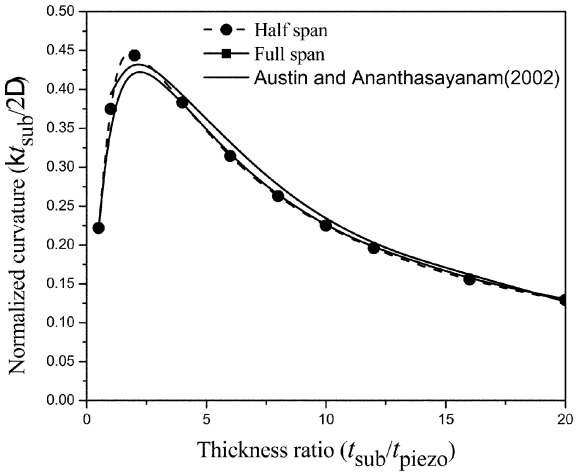

Fig. 10 Normalized curvature versus thickness ratio for modulus ratio (E_{sub}/E_{piezo}) = 1.0

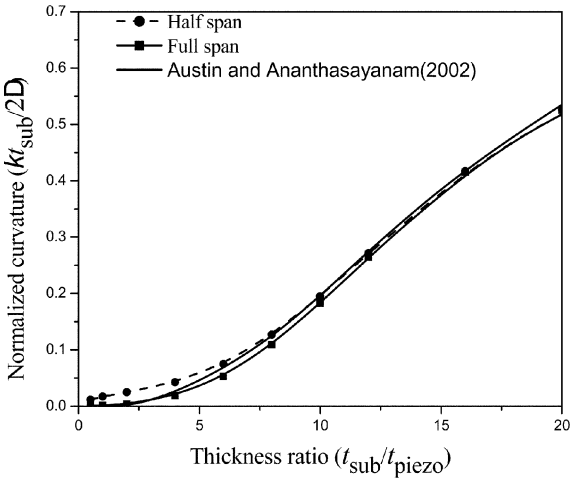

Fig. 11 Normalized curvature vs. thickness ratio for modulus ratio (E_{sub}/E_{piezo}) = 7.45×10^{-}

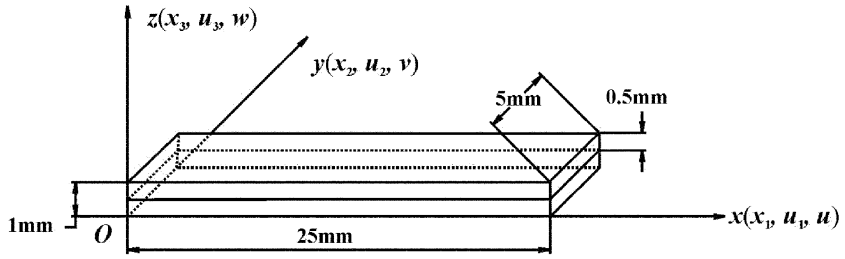

Fig. 12 Piezo-rubber beam

3.3. Both ends pinned piezo-rubber beam

In this new example, a rubber beam having one layer of piezoelectric material (PVDF) of same thickness above or below the rubber substrate with both ends pinned is studied. The dimensions of the beam are shown in Fig. 12. A downward point load is applied at the midpoint of the beam.The beam is divided into 40 elements (mesh size: 20×1×(1+1)). The boundary conditions imposed for numerical analysis are u, v, $w = 0$ at $x = 0$, $z = 0.5$ mm and $x = 25$ mm, $z = 0.5$ mm and $v = 0$ at $y = 2.5$ mm. The Mooney-Rivlin material model is used for rubber. The midpoint deflections and the sensed voltages are shown with respect to load step which is defined as the ratio of the load applied to the maximum load 0.09N in Figs. 13-16. Astress softening effect is observed from Figs. 13 and 14 when the rubber substrate is below the PVDF layer and a stress stiffening effect is seenfrom Fig. 15 and 16 when the rubber substrate is used as top layer.

3.4. A piezo-rubber cantilever beam

A piezo-rubber cantilever beam (Fig. 17) is considered in this case. The beam is made of a rubber layer and a PVDF layer. Thickness of rubber layer is 10 mm while that of PVDF layer is 0.5 mm. The

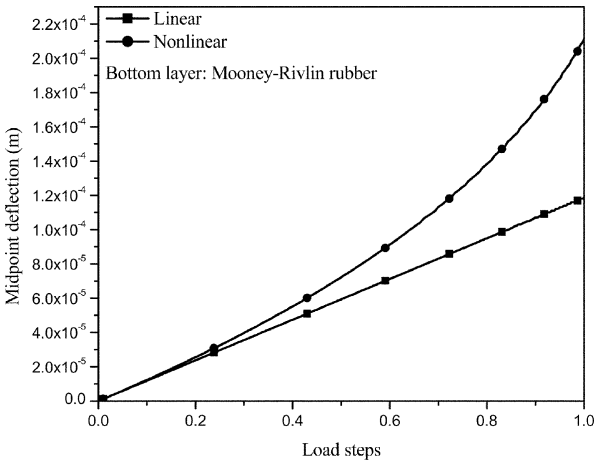

Fig. 13 Midpoint deflectionsof a PVDF rubber beam with both ends pinned

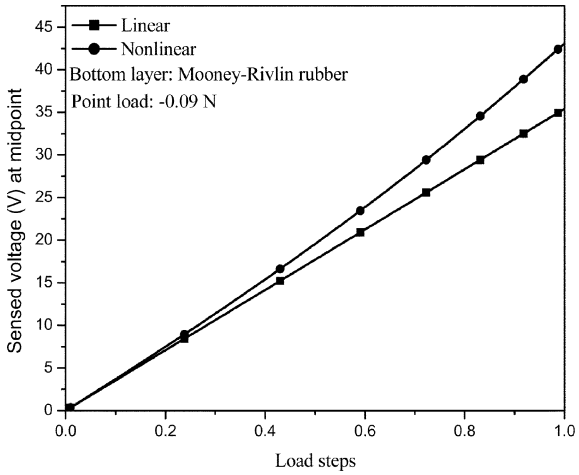

Fig. 14 Sensed voltages (V) at midpoint of a PVDF rubber beam with both ends pinned

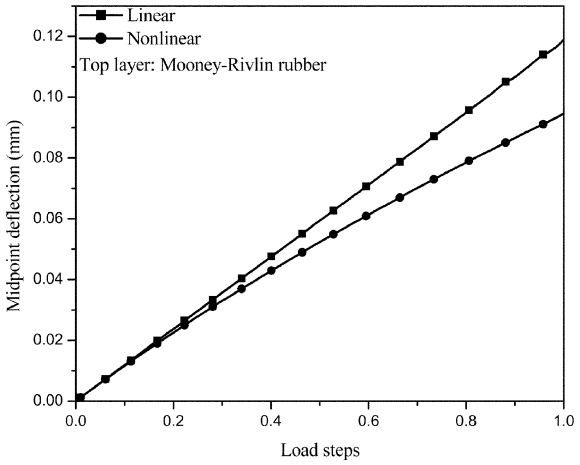

Fig. 15 Midpoint deflection of a PVDF rubber beam with both ends pinned

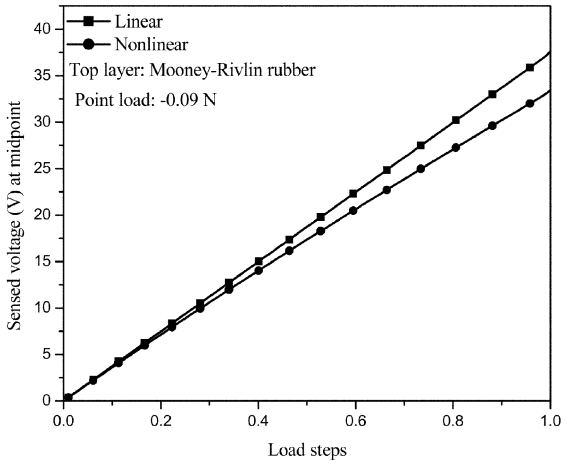

Fig. 16 Sensed voltages (V) at midpoint of a PVDF rubber beam with both ends pinned

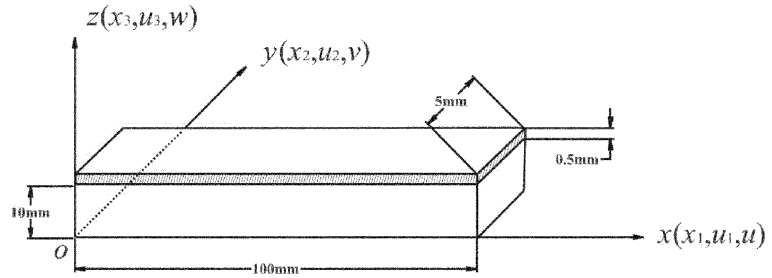

Fig. 17 Piezo-rubber cantilever beam

neo-Hookean, Mooney-Rivlin and Ogden-Tschoegl material models are used for rubber material. The study is also carried out with rubber beam with different layer combinations, i.e., top layer as PVDF

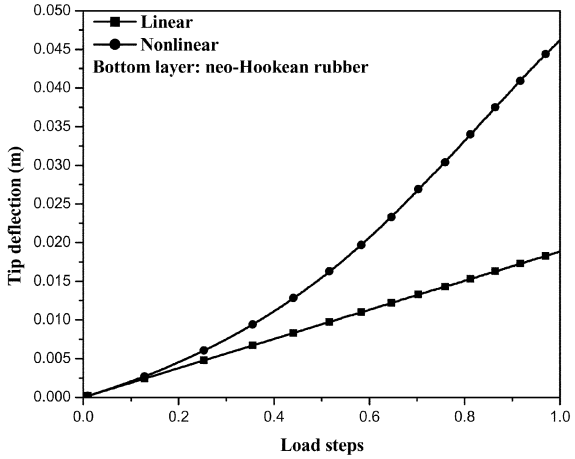

Fig. 18 Tip deflections of a cantilever piezo-rubber beam

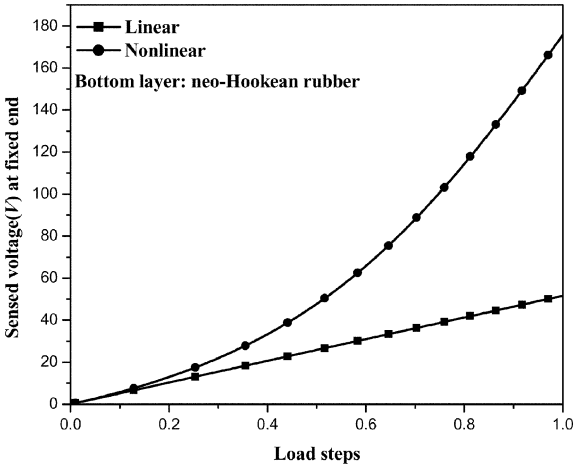

Fig. 19 Sensed voltages at the fixed end of a cantilever piezo-rubber beam

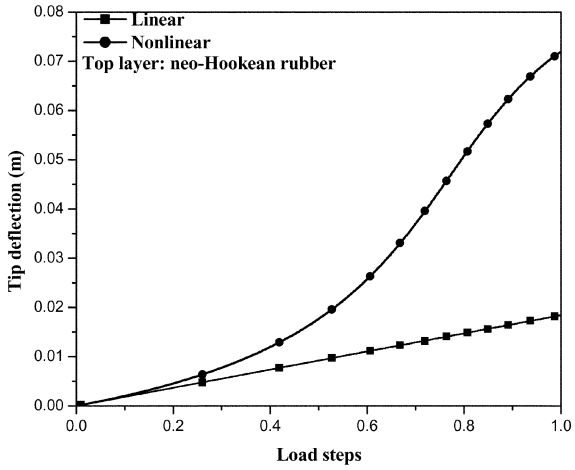

Fig. 20 Tip deflections of a cantilever piezo-rubber beam

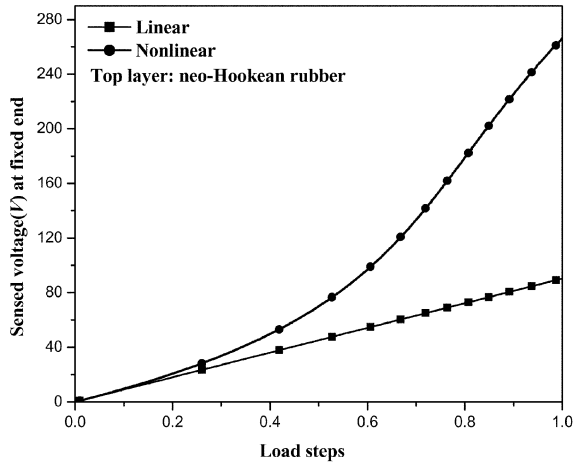

Fig. 21 Sensed voltages at the fixed end of a cantilever piezo-rubber beam

and bottom layer as rubber material or vice-versa. At fixed end ($x = 0$) all the three degrees of freedom are restrained while in the mid vertical plane ($y = 2.5$ mm) only displacements (v) along the y-direction is assigned as zero. The rubber substrate is divided into 40 elements (mesh size: 20×1×2) and PVDF layer is divided into 20 elements (mesh size: 20×1×1). Multipoint constraint is applied to calculate the sensed voltage at the fixed end element-wise. The element sensed voltages are calculated from total nodal displacements using secant stiffness matrix of individual element. Each piezo-rubber cantilever beam is subjected to tip transverse point load and a compressive tip load. The tip deflections and the sensed voltages with respect to load step which defined as the ratio of the load applied to the maximum load (maximum transverse tip load is -0.125N and maximum compressive tip load is 0.5N) at the fixed end are shown in Figs. 18-29 as new results. Due to compressive load there is stress softening effects in all the cases and sensed voltages at the root of the cantilever beam is much higher than those forlinear analysis.

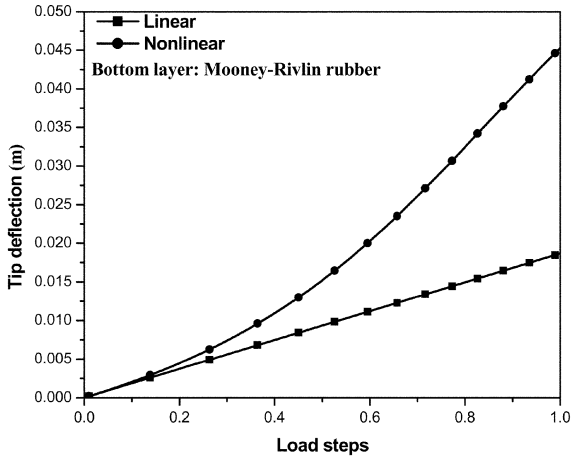

Fig. 22 Tip deflections of a cantilever piezo-rubber beam

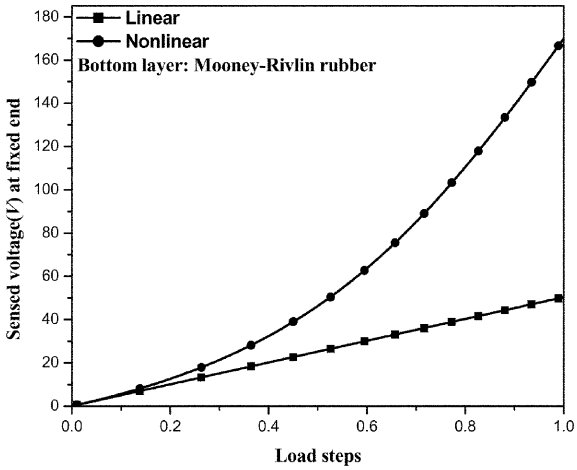

Fig. 23 Sensed voltagesat fixed end of a cantilever piezo-rubber beam

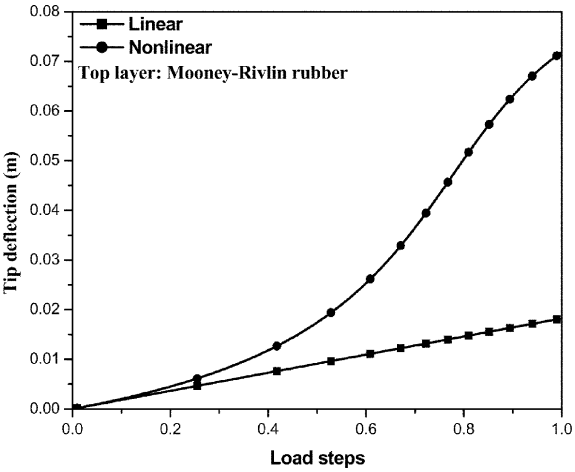

Fig. 24 Tip deflections of a cantilever piezo-rubber beam

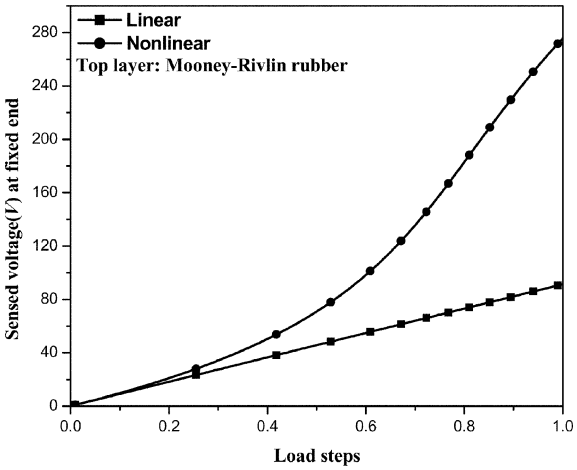

Fig. 25 Sensed voltages at the fixed end of a cantilever piezo-rubber beam

3.5. Control of a smart rubber beam with both ends pinned

In this example a smart rubber beam with both ends pinned as shown in Fig. 30 is investigated. The beam is made of three layers, the middle layer is a rubber material and the top and bottom layers are of PVDF. All the layers have equal thickness 0.5 mm. The beam is 100 mm long. The bottom layer is used as a sensor and the top layer as an actuator. The average voltage of the sensor elements is fed back to the outer surface appropriately multiplied by a gain factor. Both the sensor and actuator are divided into the segments equal to the number of divisions along the x-direction. The beam is subjected to a point downward vertical load at middle of the beam. The material properties of the sensor are Young's modulus $E = 2.0$ GPa, Poisson's ratio $v = 0.29$, piezoelectric stress coefficient $e_{31} = -0.046$ C/m^2 , and dielectric constant $\wp_3 = 1.062\times10^{-10}$ F/m and those of the actuator are Young's modulus $E = 2.0$ GPa, Poisson's ratio $v = 0.29$, piezoelectric stress coefficient $e_{31} = -0.046$ C/m^2, and dielectric constant $\wp_3 = 1.062\times10^{-10}$ F/m.

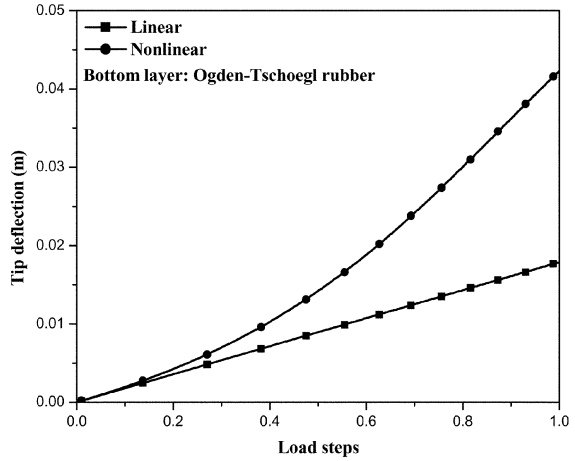

Fig. 26 Tip deflections of a cantilever piezo-rubber beam

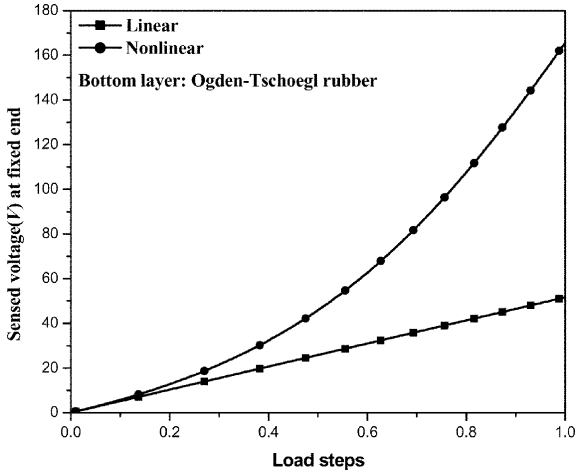

Fig. 27 Sensed voltages at the fixed end of a cantilever piezo-rubber beam

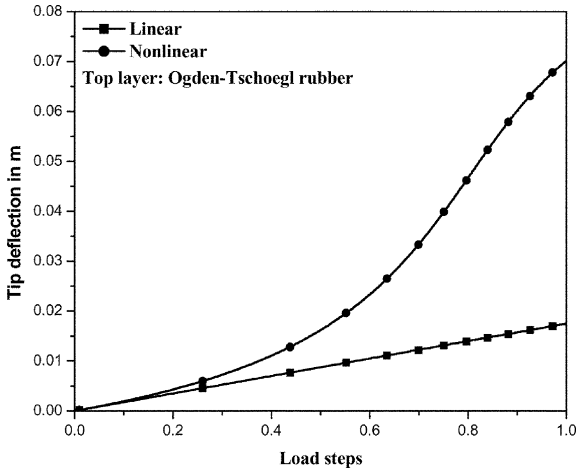

Fig. 28 Tip deflections of a cantilever piezo-rubber beam

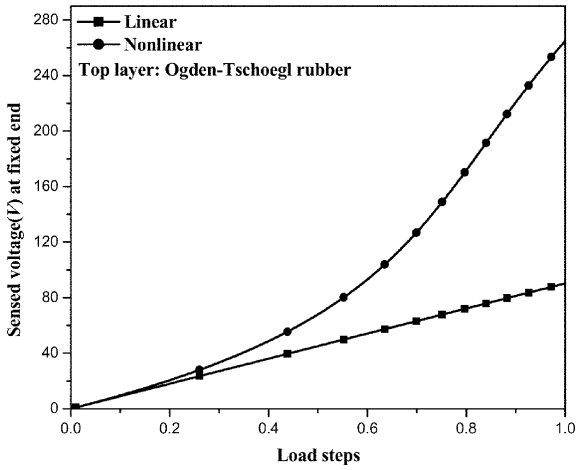

Fig. 29 Sensed voltages at the fixed end of a cantilever piezo-rubber beam

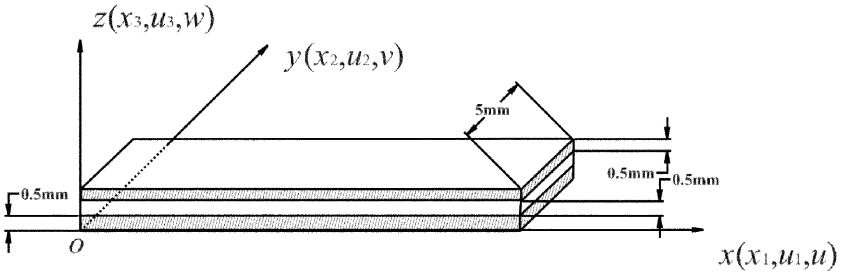

Fig. 30 A smart rubber beam

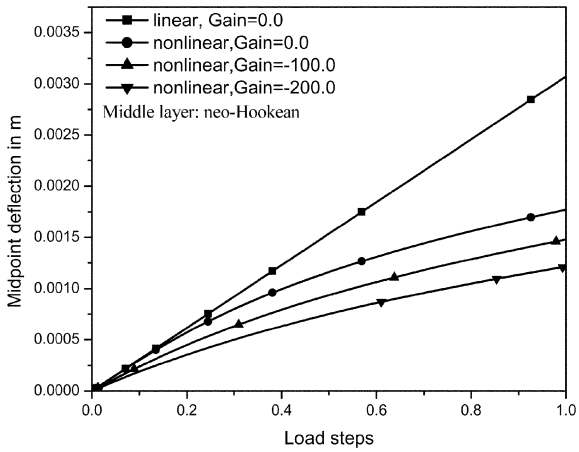

Fig. 31 Midpoint deflections of both end pinned smart rubber beam

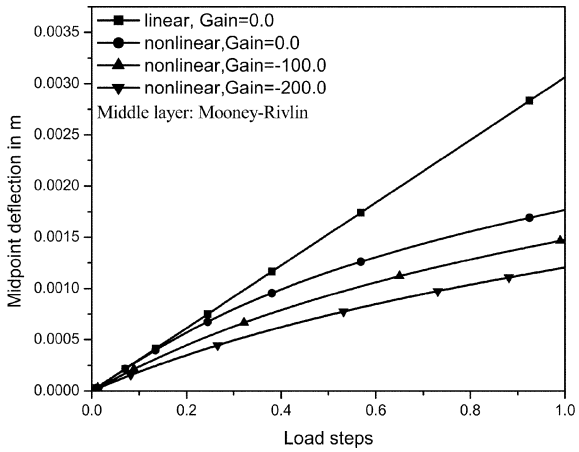

Fig. 32 Midpoint deflections of both end pinned smart rubber beam

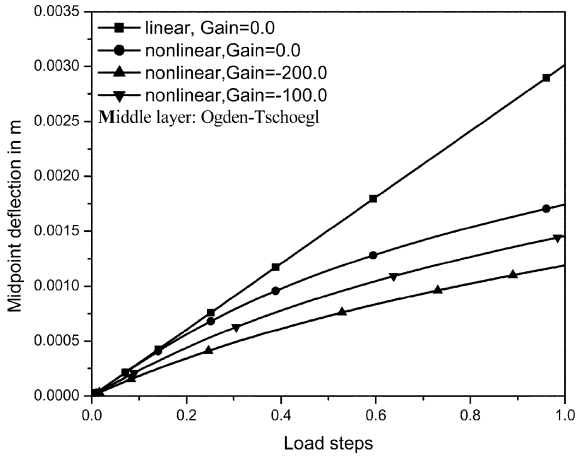

Fig. 33 Midpoint deflections of both ends pinned smart rubber beam

The mid-point deflections versus load steps (ratio of applied load to maximum load 0.25 n) are shown as new results in Figs. 31 -33for neo-Hookean, Mooney-Rivlin and Ogden-Tschoegl type rubber models, respectively. Multipoint constraints method is applied to calculate thesensed voltage at the sensor elements using secant stiffness matrix. The electrical degrees of freedom are condensed to form the elemental stiffness matrix for piezoelectric layers. A mesh division of 20×1×1 is taken for each piezoelectric layer. From the figures, it is seen that the tip deflection decreases as the feed back gain factor increases.

4. Conclusions

A finite element model using updated Lagrangian approach has been proposed for nonlinear static analysis of rubber components with surface bonded piezoelectric layers under different loading conditions. A compressible stain energy function has been utilized. A twenty node solid brick element is used to formulate the finite element model. The present formulation has been applied to PVDF

bimorph beam subject to electrical potential as well as a combination of transverse and compressive forces to validate the present formulation. The results predicted by the present formulation match well with the analytical solutions and the available published results. Then a smart rubber beam comprising piezoelectric (PVDF) and rubber layers under transverse and compressive axial forces is considered to show the stiffening and softening effects of piezoelectric material. Lastly, a beam with both ends pinned is investigated to show how the piezoelectric materials are used to control the deflections of structural components. The present method gives a straightforward and simple approach for the nonlinear analysis of rubber components with piezoelectric patches and smart rubber components.

References

Allik, H. and Hughes, T. J. (1970), "Finite element method for piezoelectric vibration", *Int. J. Numer. Methods Eng.*, **2**, 151-157.

Austin, E. M. and Ananthasayanam, B. (2002), "Modeling of piezoelectric materials on rubber beams", *Proceedings of SPIE, Smart Structures and Materials*, **4697**, 131-138.

Bailey, T. and Hubbard, J. E. (1985), "Distributed piezoelectric-polymer active vibration control of a cantilever beam", *AIAA J. Guidance, Control Dyn.*, **8**(5), 605-611.

Bathe, K. J. (1996), *Finite Element Procedures in Engineering Analysis*, Prentice Hall, Englewood Cliffs.

Chen, S.-H., Wang, Z.-D., and Liu, X.-H. (1997), "Active vibration control and suppression for intelligent structures", *J. Sound Vib.*, **200**(2), 167-177.

Crawley, E. F. and de Luis, J. (1987), "Use of piezoelectric actuators as elements of intelligent structures", *AIAA J.*, **25**(10), 1373-1385.

Crisfield, M. A. (1981), "A fast incremental/iterative solution procedure that handles snap-through", *Comput. Struct.*, **13**, 55-62.

Fanson, J. L. and Caughey, T. K. (1987), "Positive position feedback control for large space structures", *Proceedings of the 28th AIAA/ASME/ASCE/AHS/ASC Structures, Structural Dynamics and Material Conference 2B*, 588-598.

Forward, R. (1979), "Electronic damping of vibrations in optical structures", *Applied Optics*, **18**(5), 690-697.

Gent, A. N. (2001), *Engineering with Rubber*, Hanser Publishers, 2nd Edn.

Lim, C. W., He L. H., and Soh, A. K. (2001), "Three-dimensional electromechanical responses of a parallel piezoelectric bimorph", *Int. J. Solids Struct.*, **38**, 2833-2849.

Manna, M. C., Sheikh, A. H., and Bhattacharyya R. (2006), "A compressible finite element model for hyperelastic members under different modes of deformation", *Struct. Eng. Mech.*, **24**(2), 227-245.

Mukherjee, A. and Saha Chaudhuri, A. (2002), "Piezolaminated beams with large deformations", *Int. J. Solids Struct.*, **39**, 4567-4582.

Mukherjee, A. and Saha Chaudhuri, A. (2004), "Exact solutions for instability control of piezolaminated imperfect struts", *AIAA J.*, **42**(4), 857-859.

Mukherjee, A. and Saha Chaudhuri, A. (2005), "Active control of piezolaminated columns – exact solutions and experimental validation", *Smart Mater. Struct.*, **14**, 475-482.

Ogden, R. W. (1984), *Non-linear Elastic Deformations*, Ellis Horwood, Chichester.

Olson, H. F. (1956), "Electronic control of noise, vibration, and reverberation", *J. Acoustical Society of America*, 966-972, Sept.

Park, C. and Chopra, I. (1996), "Modeling piezoceramic actuation of beams in torsion", *AIAA J.*, **34**(12), 2582-2589.

Peng, S. H., and Chang, W. V. (1997), "A compressible approach in finite element analysis of rubber-elastic materials", *Comput. Struct.*, **62**, 573-593.

Tiersten, H. F. (1969), *Linear Piezoelectric Plate Vibrations*, Plenum Press, first ed., New York.

Tseng, C. I. (1989), "Electromechanical dynamics of a coupled piezoelectric/mechanical system applied to vibration control and distributed sensing", Ph. D. Dissertation, University of Kentucky, Lexington, KY.

Wood, R. D. and Schrefler, B. (1978), "Geometrically nonlinear analysis – a correlation of finite element notations", *Intl. J. Numerical Methods Eng.*, **12**, 635-642.

Ye, S., Ling, S. F. and Ying, M. (2000), "Large deformation finite element analyses of composite structures integrated with piezoelectric sensors and actuators", *Finite Element in Analysis and Design*, **35**, 1-15.

CC